
Investigation of the structural behaviour of a masonry castle by considering the actual damage

Maria E. Stavroulaki

Applied Mechanics Laboratory,
School of Architecture,
Technical University of Crete,
GR-73100 Chania, Greece
Email: mstavr@mred.tuc.gr
Website: <http://www.arch.tuc.gr/>

Georgios A. Drosopoulos

School of Civil Engineering,
University of KwaZulu-Natal,
4041 Durban, South Africa
Email: DrosopoulosG@ukzn.ac.za
Website: <http://civeng.ukzn.ac.za/Homepage.aspx>

Efstathia Tavlopoulou and Nikos Skoutelis

School of Architecture,
Technical University of Crete,
GR-73100 Chania, Greece
Email: efstathia.tavlopoulou@gmail.com
Email: nskoutelis@isc.tuc.gr
Website: <http://www.arch.tuc.gr/>

Georgios E. Stavroulakis*

School of Production Engineering and Management,
Technical University of Crete,
GR-73100 Chania, Greece
Email: gestavr@dpem.tuc.gr
Website: <http://www.comeco.tuc.gr/>
*Corresponding author

Abstract: The structural behaviour of Frangokastello, a mediaeval masonry castle located in Crete, Greece is studied. The structure presents several damaged areas, consisting of cracks and local failure of masonry. The finite element method (FEM) is used to investigate how the existing failure of the structure affects its mechanical response. First, an eigenvalue analysis of the structure without the cracks and a dynamic modal analysis are done. Then, a non-linear constitutive model using a smear crack law is used to investigate the limit state of the structure under static and dynamic loading. Finally, unilateral contact interfaces are introduced, to simulate the cracks which appear in the

structure. This model, which consists of several non-linearities, is tested under non-linear time history analysis. Comparison of the results demonstrates how the pathology of the structure affects its response. This procedure is necessary towards taking actions for the reinforcement of the structure.

Keywords: masonry; crack; dynamic analysis; unilateral contact; finite element analysis; modal analysis; time-history analysis of structures; rehabilitation of monuments; structural evaluation of damaged structures.

Reference to this paper should be made as follows: Stavroulaki, M.E., Drosopoulos, G.A., Tavlopoulou, E., Skoutelis, N. and Stavroulakis, G.E. (2018) 'Investigation of the structural behaviour of a masonry castle by considering the actual damage', *Int. J. Masonry Research and Innovation*, Vol. 3, No. 1, pp.1–33.

Biographical notes: Maria E. Stavroulaki received her Diploma in Civil Engineering from Aristotle University of Thessaloniki, in 1988, and PhD from Technical University of Crete, in 1996. She is an Assistant Professor at the School of Architecture, since 2013. She was a Lecturer in the Department of Sciences, since 2005. She supervised or co-supervised several Master and Doctoral Theses, and published two books, several contributions in international journals, books and conferences. The main part of her scientific research refers to structural engineering of masonry structures (analysis, design, dynamics, earthquake stability) and computational mechanics for heritage structures (finite elements, contact mechanics, restoration, strengthening).

Georgios A. Drosopoulos obtained his Diploma in Civil Engineering from National Technical University of Athens, in 2002, and his PhD from University of Ioannina in 2006. After a post-doctoral stay at Leibniz University of Hannover, and Technical University of Crete, he was appointed as a Senior Lecturer in Civil Engineering, University of KwaZulu-Natal, South Africa in 2016. He has published several papers in international journals, books and conferences. His research activities focus on contact mechanics, multi-scale computational homogenisation for composites, auxetic materials and masonry, non-linear finite elements for steel structures under normal and elevated temperatures, etc.

Efstathia Tavlopoulou obtained her Architectural Engineering Diploma and Master of Science in Engineering and Technology of Materials and Structures, both from the Technical University of Crete, in 2012 and 2015, respectively. A paper based on her Master's Thesis was published at the proceedings of *8th GRACM International Congress on Computational Mechanics* in 2015. Currently, she is a PhD candidate at National Technical University of Athens, in the Department of Mechanical Engineering, on Smart Materials.

Nikos Skoutelis graduated from I.U.A.V. – Venice in 1987 and received PhD from N.T.U.A. in 2006. He has worked, in collaboration with Flavio Zanon, in Venice from July 1987 and in Heraklion since 1993, on public and private projects, at the same time participating in architectural competitions. His theoretical works concern architecture and the city of the renaissance; the theory of restoration and the contribution of history as a tool in architectural composition. Since 2005, he has been teaching Architectural Design in the Department of Architecture of the Technical University of Crete, where he was elected Associate Professor in 2007.

Georgios E. Stavroulakis obtained his Civil Engineering Diploma and PhD, both from the Aristotle University of Thessaloniki in 1985 and 1991, respectively, as well as the 'venia legendi' in Mechanics from the Carolo Wilhelmina Technical University of Braunschweig in 2000. He was an Associate Professor of Mechanics in University of Ioannina, 2000–2005 and Professor in, Technical University of Crete, since 2005. He is Visiting Lecturer (Privatdozent) at the Technical University of Braunschweig, and Honorary Professor at Jordan University of Science and Technology. He works on computational mechanics, nonsmooth mechanics, optimisation and applications.

1 Introduction

Frangokastello fortress, as defence infrastructure, has been a key point for the victory of the Venetians in the area of southern Crete against pirates and local feudal lords. After the first phase of operation, there are no historical documents likely to reveal a constant concern on the part of the Venetian authorities and 200 years after its construction, only the period between 1593 and 1597, General Prudent of Crete, Nicolo Dona, refers to the deterioration of the building, due abandonment. In 1610, 13 years later, the engineer army Rafaele Monanni, mentions the fortress as uninhabited. Other Prudent, Lorenzo Contarini in 1634, predicted to be projects, but to no avail, which bears in 1644 by Andrea Corner, again without complete restoration of damage due to lack of money. As a result, from 1645 until the Orlov, there are no sources to report news about the fortress. The removal of the wooden beams of the floors and the cornerstones of southern special towers is a fact that constantly comes up during other historical periods.

However, the intervention of the Ottomans, after the revolution of 1866, has been significant, where 66 battlements were opened, taking as a running surface for the soldiers, the ruins of the roofs in the ground floor areas. Also a significant intervention was the impairment of the wall thickness in the three small towers, in order to achieve the creation of advanced rifle boxes in these parts of the fortress. The rifle boxes, reduction of wall thickness, with the simultaneous opening of the eastern entrance, are the most active interventions after the manufacturing of the structure in the 14th century.

Advanced numerical analysis, could offer significant information both for the understanding of the causes of existing damage and for the design of adequate design of strengthening according to Betti et al. (2011). Finite element method (FEM) and 3D models were used by Milani et al. (2012) for comparison between present structural situation and hypothetical original configuration of the Maniace castle in Syracuse, Italy and by Tiberti et al. (2016) to study the Finale Emilia castle behaviour under 2012 Emilia Romagna seismic sequence. Cattari et al. (2014) presented the seismic vulnerability of mediaeval fortresses at the Emilian which is high mainly due to constructive and dynamic features. Starting from the analysis of the geometrical and constructive features, the interpretation of their seismic vulnerability has been based on an accurate damage assessment and supported by the numerical results of typical configurations. Specific the towers have shown a different seismic response because of: the different interventions they were subjected to; the different position in plan and connection level with the

perimeter wall (which determined irregularities in plan and in elevation) and the different quality of connection with the other fortress structures.

The use of some interfaces along the lines where cracks and other damage are appeared, is a promising alternative according to Stavroulaki and Stavroulakis (2002). The study of several damage scenario of the Plaka stone bridge in Epirus, Greece, was done by Stavroulaki et al. (2002) and Stavroulaki (2004), using unilateral contact models along interfaces, and the comparison with a model using the theory of continuum damage mechanics, under static loads, gave good correlation between the two models. The same conclusion was extracted from research of Ford et al. (2003). These interfaces were modelled by using the unilateral contact models of currently available general purpose finite element programs (like MARC). Furthermore, Betti et al. (2008) used the unilateral contact interfaces for the assessment of failure of masonry arches.

In this paper, the structural analysis of the Frangokastello fortress was done by the FEM. For the modelling the existing geometry, the history of the monument, the quality of building materials and subsoil conditions were considered. To investigate the way that structural failures affect the structural behaviour of the masonry castle, the existing cracks and faults like disorganisation of the material were considered in our analysis. Cracks were simulated by the technique of unilateral contact interfaces between contact bodies.

First, modal analysis was done in order to calculate the main frequencies of the structure. In continue, spectral analysis was done for the design spectrum, according to the Greek regulation. Finally, transient dynamic analysis for various base excitations corresponding to different earthquakes was done for all the examined models and the critical areas of the structure were estimated. The activation of contact mechanisms lead to modification of the load transfer mechanisms and in particular to local reduction of the maximum displacement but also to the appearance of higher maximum values in different locations of the structure.

2 Present condition of the structure

The Frangokastello castle consists of three small towers and a third bigger with height equal to 9 m and 15 m accordingly and four perimeter walls. A plan view of the castle follows, which indicates the main dimensions and the position of the damages (Figure 1).

The major damage is located on the Northwestern tower, and is visible with a vertical crack which runs the north side and creates an opening of a few centimetres. The crack appears along the entire height of the tower (Figures 2–4). It is a bending tensile crack, out of plane bending of the wall, in combination with the tower turning as shown at the results of the analysis.

Another, through crack with smaller opening appears along the entire height of the east wall of the structural core (Figures 5 and 6). This crack is also due to out of plane bending of the wall of free height of ~8 m and 1.25 m average thickness. Notably the corresponding, western, perimetric wall of the fortress, of shorter length and larger average thickness (1.4 m) does not display similar failure.

Figure 1 Plan view of the carrier and major structural damages (see online version for colours)

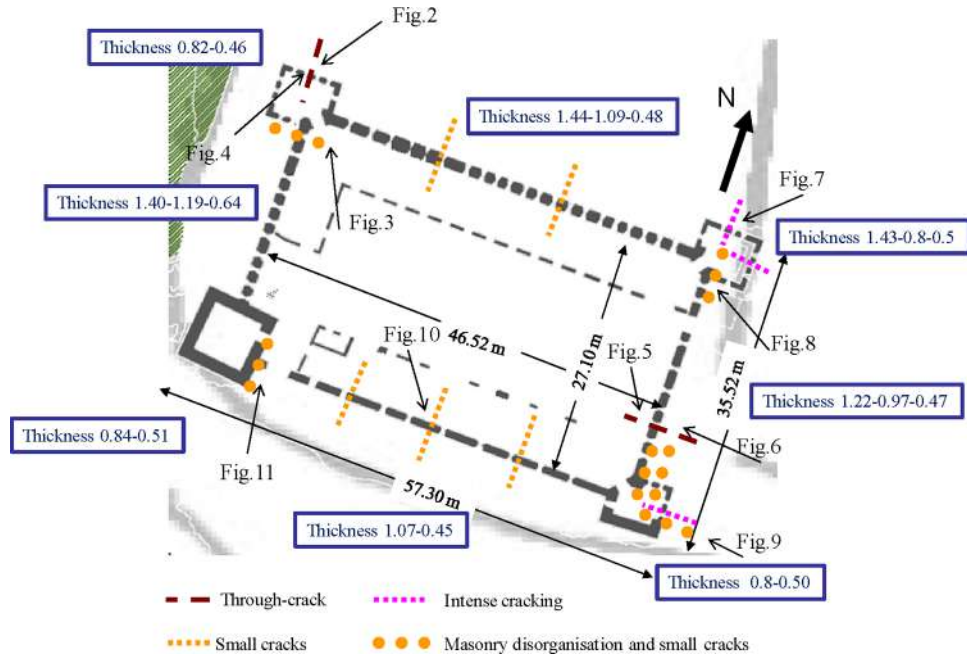


Figure 2 North West tower: east side (see online version for colours)



Figure 3 North West tower: entrance (see online version for colours)



On the north side of the north east tower (Figure 7), another crack appears (partially refurbished), where we can observe the phenomenon of the disruption of the masonry (Figures 8).

Figure 4 Large bright, vertical crack in the north facade, of the NW tower (internal view) (see online version for colours)



Figure 5 Vertical, through and through crack in the east wall: external view (see online version for colours)



Figure 6 Vertical, through and through crack in the east wall: internal view (see online version for colours)



Figure 7 Crack in the north face, north east tower (see online version for colours)



Figure 8 Disruption of the masonry in the south side, north east tower (see online version for colours)



We can observe similar behaviour to the southeast tower, with cracks on the east side (Figure 9) and disruption of the masonry at lower levels. The cracks in this specific region are due to the out of plane bending of the masonry and shear failure, which begins from the opening and appears at the region, where we have reduction of the cross-section (see, architectural plans, where the south wall's thickness is 1.4 m and the east and north wall's is 0.77 m).

Smaller cracks appear on the south wall (Figure 10), due to out of plane bending (according to the analysis). At the same time, lower on the south wall and at the area which is connected to the tower (Figure 11), we can detect strong disruption of the masonry.

The north wall and the southwest tower are in good condition, without any significant damage, in terms of cracks or the disruption of the material are concerned. Local problems can be solved by the restoration of the continuity of the material.

Figure 9 Cracking and disruption of the masonry, in the east side, south east tower (see online version for colours)



Conclusively:

- The presence of small cracks in the foundation soil contributed to the strengthening of the seismic load of the structure. As a result, cracks in weak parts of the structure appeared, such as the walls of the small towers and the southern and eastern wall.
- The reduction of the wall thickness of the towers to the low level in the period from 1883 to 1886, aided by the opening of the rifle boxes, resulted in a decrease of the strength of these structures in seismic stress, as a result (as mentioned above), the through and through cracks.
- The destruction of the intermediate buildings of the barracks and the floors in the towers (horizontal diaphragms), led to the increase of the free height of the outer walls and thus, to the development of bigger oscillations.
- The walls and their depended horizontal surfaces, that have not been modified, have kept their original structure.
- The walls and the surfaces, that despite the reduction of their size, were sealed with new mortar, during the construction period from 1883 to 1886, maintained their good condition.
- Restoration works periods from 1972 to 1974, 1992 and in 2006, although not in line with modern principles of intervention in historical sites, were able to avoid further damage.
- The lintels of reinforced concrete led to the creation of small cracks, after strong earthquakes, but after moderate earthquakes they acted positively, in terms of the static behaviour of the core. Stavroulaki and Liarakos (2012) to study the unilateral contact effects (i.e., separation, sliding) between the lintels of reinforced concrete

over the openings and the masonry wall, a parametric non-linear dynamic analysis was done. From the analysis, it is shown that the influence of this reinforcement on the dynamic response of masonry structures depends on many parameters like the magnitude of the ground motion and the friction coefficient of the interface between the lintels and the masonry. The positive effects of contact mechanisms can be reduced in case of a strong motion where topical relief, in parallel with stress concentration to other places, appears.

Figure 10 Disruption on the top of a south wall, internal view (see online version for colours)



Figure 11 Disruption of the masonry, in the connection area between the south wall and the south west tower (see online version for colours)



3 Structural finite element analysis

3.1 Mechanical properties of the masonry

To create the computational model and to assess the structural ability, the properties of the materials have been estimated from laboratory measurements on material samples, of non-structural elements, taken from the area of manufacture.

Coring is considered to be a particularly reliable, semi-destructive method, where several cores, of cylindrical shape, are extracted from the test component with penetration. This procedure allows determining – among others – the compressive strength, Young’s modulus, Poisson ratio of the stone. The laboratory measurements were conducted in collaboration with the Laboratory of Mechanics of School of Mineral Resources Engineering, Technical University of Crete.

From the compression test on several, different stone samples (see Figure 12) and the appropriate processing, the following values were obtained for the Young’s modulus (Table 1) and the compressive strength (Table 2).

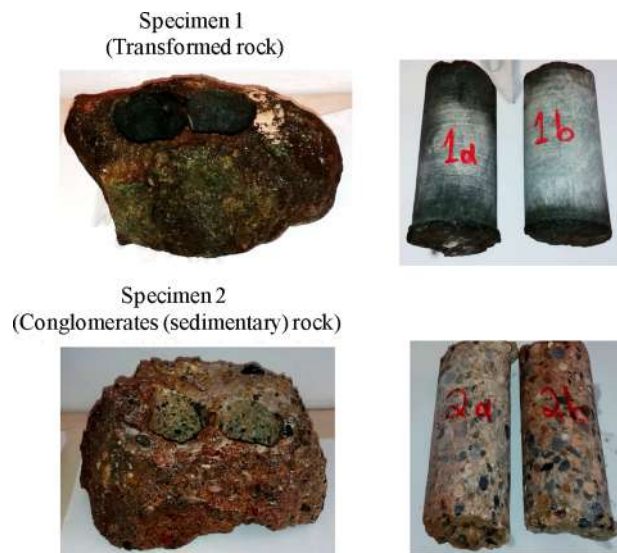
Table 1 Young’s modulus from compression test on several samples

Specimen	1a	1b	2a	2b
E (GPa)	54.19	42.95	34.68	25.40

Table 2 Compression test on several stone samples

Specimen	1a	1b	2a	2b
fk (MPa)	126.46	103.86	46.08	37.44

Figure 12 Two of the stone samples from which the specimens were extracted (see online version for colours)

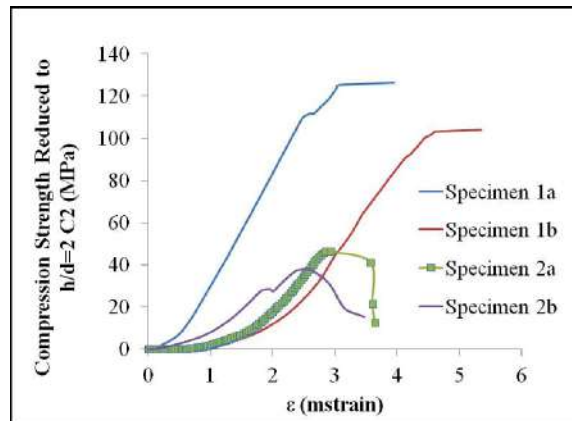


As depicted below, the value of Young's modulus, which was finally used in the analysis, according to the requirements of Eurocode 6 (EN1996), is equal to 21.15 GPa.

To investigate the non-linear behaviour of the core, compression tests were conducted again, on samples of stones. Figure 13 shows the stress-strain diagrams of uni-axial compression, of different components.

For the compressive strength of the stone, the average of the experimentally measured values was found (Table 2): 78.46 MPa.

Figure 13 Stress-strain diagrams of uni-axial compression, of different components (see online version for colours)



The hydraulic character of the mortars was principally responsible for the adequate preservation condition of mortars and plasters. The major coating removal was observed in the southern wall, where the weathering conditions are very aggressive. Therefore, the masonry and the mortars are still functional and any significant corruption or cracks are mostly attributed to mechanical faults or violent historic devastations of the castle rather than the mortar manufacturing condition. So except the specific areas the main problem of the materials is the surface erosion.

For the mortar, an average compressive strength equal to 10 MPa value was estimated based on its composition.

Therefore, based on the Eurocode 6, national Annex, the characteristic value of compressive strength of the masonry is: $f_{ck} = 0.5 \times 78.46^{0.7} \times 10^{0.3} = 21.15$ MPa.

And the characteristic value of tensile strength of the masonry is:

$$f_{tk} = 0.09 \times f_{ck} = 1.90 \text{ MPa} \quad (0.03 f_{ck} \leq f_{tk} \leq 0.09 f_{ck}).$$

Overall, the final elastic properties, which were selected are:

Young's modulus $E = 21.15$ GPa ($=1000 \times f_{ck}$)

Poisson ratio $\nu = 0.25$

Mass Density: $\rho = 2000$ kg/m³.

Shear measure $G = 8.46$ GPa ($=0.4 \times E$)

Compressive strength $f_{cd} = f_{ck}/\gamma_M$, where $\gamma_M = 2.7 \times 2/3 = 1.8$, therefore

$$f_{cd} = 21.15 / 1.8 = 11.75 \text{ MPa.}$$

Tensile strength $f_{td} = f_{tk} / \gamma_M = 1.90 / 1.80 = 1.06 \text{ MPa.}$

For the wooden beams of the floors, of the south-western tower, the following mechanical properties were selected:

Young's modulus $E = 9.807 \text{ GPa}$

Poisson ratio $\nu = 0.25$

Mass density: $\rho = 600 \text{ kg/m}^3$.

Additionally, comparison with empirical formulas that have been proposed by Tassios and Chronopoulos (1986), in which the proportion of mortar (joint) to masonry volume, the quality of masonry surface, the size of the stones and the mortar joints are taken into account, reveals that the values of the mechanical properties are very close to those obtained by the regulation. For instance, the compressive strength of the masonry $f_{wc} = 9.91 \text{ MPa}$, which is defined as follow, is very close to the value which considered in our analysis ($f_{wc} = 11.75 \text{ MPa}$, Table 3) and it was based on the Eurocode 6:

$$f_{wc} = \xi(2/3 \times (f_{bc}^{1/2}) - \alpha) + \beta \times f_{mc} = 9.91 \text{ MPa}$$

where, f_{bc} compressive strength of stone (78.46 MPa); f_{mc} compressive strength of mortar (10 MPa); $\alpha = 0.5$ for large stones 2.5 for gravel; $\beta = 0.5$ cooperation factor of stone-mortar (0.5 for rough surfaces (like the building under study)) and 0.1 (for very smooth surfaces); ξ = factor associated with the adverse effects of thick mortar joints; $\xi = 1/[1 + 3.5(k - k_o)] \leq 1$, where $k = (\text{joint volume})/(\text{masonry volume})$ and $k_o = 0.3$.

Table 3 Mechanical properties of masonry

Material	Young's modulus E (GPa)	Yield stress (MPa)	Compressive strength f_{cd} (MPa)	Tensile strength f_{td} (MPa)	Shear strength f_{sh} (MPa)
M1	21.15	3.53	11.75	1.06	4.8
M2	20.36	2.81	11.31	0.7	4.63
M3	14.63	2.70	8.13	0.5	5.95

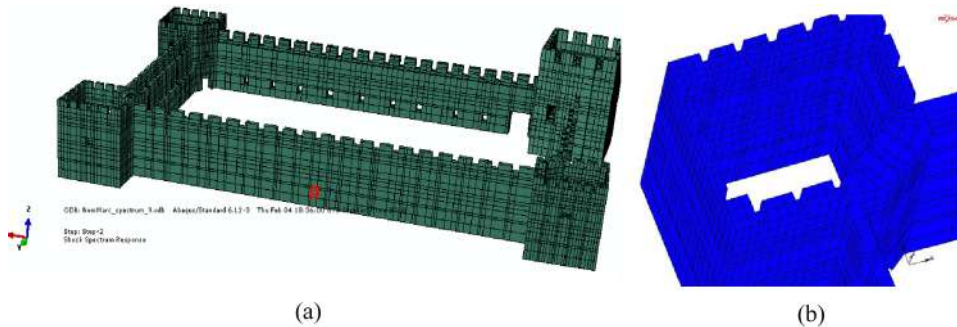
From the classification of building stones of the Frangokastello Castle which was presented by Cheimonas et al. (2016), the percentages % of the mortar, for the two typical areas of the structure are 31.73% and 40.18%, respectively, with an average value of 35.95%. These results were derived from a first statistical approach of rock fractions, which composed the structural stones at the construction of the castle, which was performed in parallel with the geophysical prospecting, that took place in and around the castle, for the determination of the main zones of discontinuities of the carbonate layer, of several metres of thickness.

Considering the major structural damages (like cracks, masonry disorganisation) different finite element models was used in order to model these damages. The mechanical properties which were used are given in Table 3.

3.2 Finite element models

For the evaluation of the mechanical behaviour of the core the FEM was used, which is appropriate for the simulation of monumental constructions, with special geometry, stiffness and mechanical behaviour, which can hardly be simulated with simplified models, according to existing research such as Spyrakos (1995), Lourenço (2002) and Leftheris et al. (2006). Thus, a model was created, consisting of 16743 three-dimensional finite elements (Figure 14(a)). The finite elements are 8-node solid elements (hexahedrons) with three transformed degrees of freedom at each node. Across the wall thickness three elements are considered at the base and only at the upper part of the walls they reduced to two (Figure 14(b)). The finite elements mesh was selected after some tries to achieve the best possible simulation of the real structure and the accuracy of the results.

Figure 14 (a) The mesh of finite elements (Model 1) and (b) detail of finite element mesh across the wall thickness (see online version for colours)



For the simulation, we took under consideration the architectural mapping, the pathology of the elements of the structure and the mechanical properties of the materials, as they have already mentioned above.

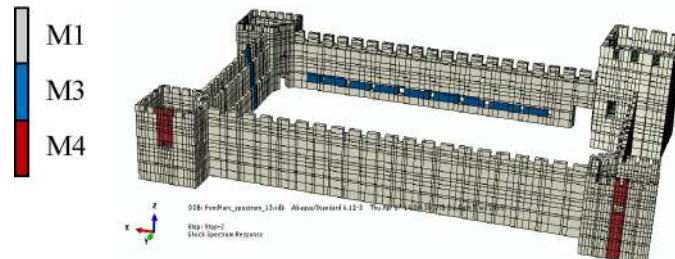
Two different general purpose finite element programs were used: The Abaqus for Models 1 and 2 which were used for modal and spectra analysis and the MSC/Marc for Models 1, 3–6, which were used for the non-linear transient analysis of the structure.

Analytically the following models were created:

Model 1: The state of the body, before the failures, assuming an average quality of material around the structure (M1 from Table 3) as shown in Figure 14.

Model 2: The present condition of the structure considering the extensive cracking areas and faults material with much lower modulus of elasticity and strength (Figure 15). Specifically for the region of large fracture (north side) of the North-Western tower and the smallest crack (north side) of north-eastern tower the modulus of elasticity was considered equal to 10 GPa (M4). For the remaining cracks and areas of intense disorganisation of the masonry, modulus equal to 14.63 GPa (M3) was considered.

Figure 15 Finite element mesh with different material to areas with extensive cracks (red for M4) and intense disorganisation of the masonry (blue for M3), (Model 2) (see online version for colours)



Model 3: The present condition of the structure considering the main cracks of the structure which were modelled by unilateral contact along interfaces where separation and frictional effects are considered (see Section 3.3). Average quality of material around the structure, (M1) was assumed and for the region of large fracture (north side) of the north-western tower, material with much lower modulus of elasticity and strength (M2) was considered (Figure 16).

Models 4, 5, 6: The present condition of the structure considering the extensive cracks of the structure (as Model 3). Average quality of material around the structure, (M1) was assumed and for the regions of the large fracture (north side) of the north-western tower, the south wall, the east and north wall of the South-East tower and the north wall of the north eastern tower, material with much lower modulus of elasticity and strength (M2) was considered. Additional lower quality of material was used (M3) for a specific area around the large fracture (north side) of the north-western tower with intense disorganisation of the masonry (Figure 17). Different parameters of friction were assumed for the three models 4, 5 and 6 (Table 4).

Figure 16 Finite element model with different material to the area with extensive crack (grey for M2) and considering the main cracks of the masonry (red lines), (Model 3) (see online version for colours)

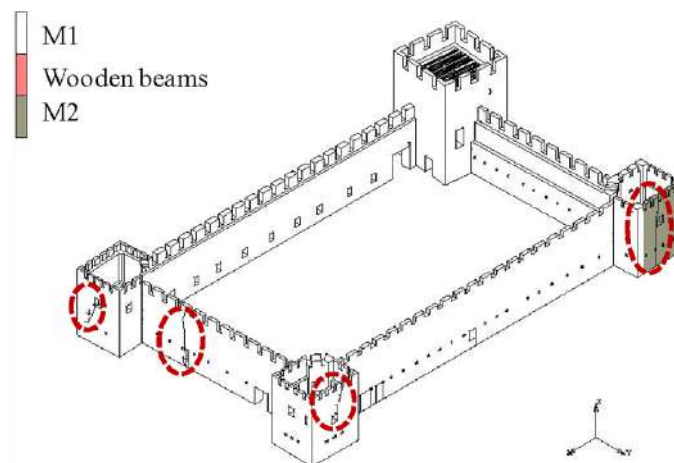


Figure 17 Finite element model with different materials to the area with intense disorganisation of the masonry (grey for M2 and black for M3) and considering the main cracks of the masonry (Models 4, 5 and 6) (see online version for colours)

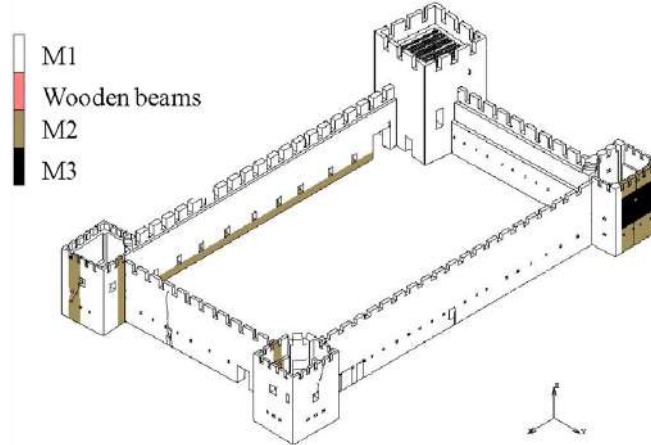


Table 4 Parameters of friction for the finite element models

Model	Friction coefficient (μ)		Friction stress limit (σ_t^{limit} (MPa))	Separation stress (MPa)
	Small cracks	Large crack		
3	0.6	0.4	1	0.61
4	0.6	0.4	1	0.50
5	0.1	0.1	1	0.00
6	0.001	0.001	0	0.00

Milani et al. (2013) present a methodology for the characterisation of the ultimate response of quasi periodic masonry. Two model were used, the first considering a heterogeneous material and the second model considering a homogeneous material obtained through the proposed homogenisation procedure. In our application, the material of masonry has been considered as homogeneous and isotropic. The generalised Mohr-Coulomb model developed by Drucker and Prager, the Mohr-Coulomb Parabolic material model was used for the masonry which describes elastic-plastic behaviour based on a yield surface that exhibits hydrostatic stress dependence. Such behaviour is observed in a wide class of soil and rock-like materials. For the wooden beams an elastic material was considered.

The cracks were modelled with unilateral contact along specific interfaces which were assumed at the place where the main cracks exist (as it is described in the next paragraph).

About the boundary conditions the whole structure supports its gravity loads and the nodes of the base are considered to be fixed with the ground since no signs of slip or movement phenomena exist to the structure.

3.3 Unilateral contact interface

3.3.1 Introduction

The possibility that some separation appears between two parts of a structure coming into contact is known as the unilateral contact phenomenon. This is a typical variable-structure nonlinearity, which involves decisions in the mechanical model. The frictional stick-slip nonlinearity is a contact – separation phenomenon. Both problems belong to the area known as non-smooth mechanics. The reason is that the arising models (functions) are non-differentiable in the classical sense.

Unilateral contact along interfaces is a suitable model for non-linear analysis of masonry structures. A number of potential interfaces are defined and along these interface separation and frictional effects are considered. The actual state at each point of the interface will be found after the solution of the problem. In case of unilateral contact and friction, algorithms have been proposed and modern general-purpose finite element software (like the MARC which is used for this study) can be used for the solution real-life problems. Effective use of the available models for the static and dynamic analysis of stone structures with unilateral frictional joints (interfaces), the successful numerical solution and the estimation of the limits of their applicability require some theoretical knowledge.

3.3.2 Description of unilateral frictional contact problem

The analysis of contact behaviour is complex because of the requirement to accurately track the motion of multiple geometric bodies, and the motion due to the interaction of these bodies after contact occurs, including the representation of the friction between surfaces. The numerical objective is to detect the motion of the bodies, apply a constraint to avoid penetration and apply appropriate boundary conditions to simulate the friction behaviour. Therefore, a constraint minimisation problem has to be solved where the constraint is the ‘no penetration’ constraint. In general, the frictionless contact problem can be represented by the minimisation problem:

$$\begin{aligned}
 &\text{Minimise} && \Pi(u) \\
 &\text{subjected to} && h_j(u) \leq 0 \quad j = 1, \dots, m \\
 &&& \text{if } Ft_i \leq f(\mu, Fn_i, v_r) \Rightarrow \text{no sliding} \quad i = 1, \dots, n \\
 &&& \text{if } Ft_i > f(\mu, Fn_i, v_r) \Rightarrow \text{sliding occur} \quad i = 1, \dots, n
 \end{aligned}$$

where $\Pi(u)$ the total potential energy of a discretised system of elastic bodies, $h_j(u)$ are inequalities which represents the inter-penetration of the bodies (if $h_j(u) \leq 0$ there is no penetration, and when $h_j(u) > 0$ there is inter-penetration of the bodies), Ft_i the tangential forces vector and $f(\mu, Fn_i, v_r)$ a function of friction coefficient, normal forces vector and relative sliding velocity, respectively. The total number of nodes in contact area is m and n is the number of increments.

During contact the resultant force transmitted from one surface to another through a point of contact is resolved into a normal force F_n , acting along the common normal, which generally must be compressive, and a tangential force F_t in the tangent plane sustained by friction. According to a regularised form of the Coulomb friction model

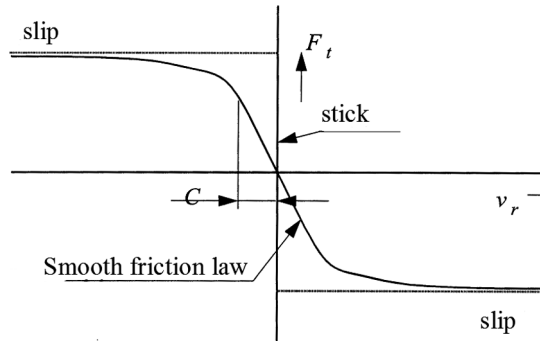
(Figure 18), the magnitude of F_t must be less than, or in the limit, equal to the force of limiting function:

$$\text{if } Ft \leq \frac{2 \cdot \mu \cdot Fn}{\pi} \arctan\left(\frac{v_r}{C}\right) \Rightarrow \text{no sliding}$$

$$\text{if } Ft > \frac{2 \cdot \mu \cdot Fn}{\pi} \arctan\left(\frac{v_r}{C}\right) \Rightarrow \text{sliding occurs.}$$

where v_r is the relative sliding velocity and C is the relative sliding velocity below which sticking is simulated. The relative sliding velocity is a constant used to smoothen the transition between the stick and no-stick conditions. The slip force is a function of the relative velocity and the input constant. The larger the value, the smaller the force required to generate slip.

Figure 18 Coulomb friction model including relative sliding



The computation of Coulomb friction in a contact problem can be based on either nodal stresses or nodal forces.

For the solution of the contact problem the direct constraint method is used for the following application. In this procedure, the motion of the bodies is tracked and when contact occurs, direct constraints are placed on the motion using boundary conditions, both kinematic constraints on transformed degrees of freedom and nodal forces. The constraint imposed is to insure that penetration does not occur. In our model these constraints are modelled by the definition of tying relations for displacement components of the contacting nodes.

Within the MARC, the unilateral contact mechanism is considered in an exact way and solved by an iterative solution method. The following must be defined:

- the contact bodies which describe the boundaries of interfaces (Figure 20)
- the contact tolerance in order to have realistic results
- the area in which the contact possibly occurs which is used in case where we know from the beginning where contact will be and in order to reduce the computation time

- the contact procedure
- the separation procedure defining the separation criterion which can be based on normal stress or normal force
- the friction model.

When a node contacts a deformable body, the average of the coefficients for the two bodies is used. The friction stress limit (σ_t^{limit}) is used to bound the maximum friction stress, based on the assumption that the extrapolated and averaged shear (friction) stress in a node is proportional to the applied shear (friction) force (see Figure 19). If the shear stress reaches the limit value, then the applied friction force is reduced, so that the maximum shear stress is given by $\min\{\mu \sigma_n, \sigma_t^{\text{limit}}\}$, where σ_n is the normal stress, according to MARC theoretical manual (MARC Analysis Research Corporation, 1997). The parameters of friction model which were used are given in Table 4.

Figure 19 Friction stress limit used by bilinear model from the MARC theoretical manual

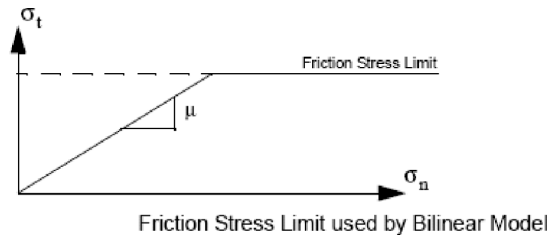
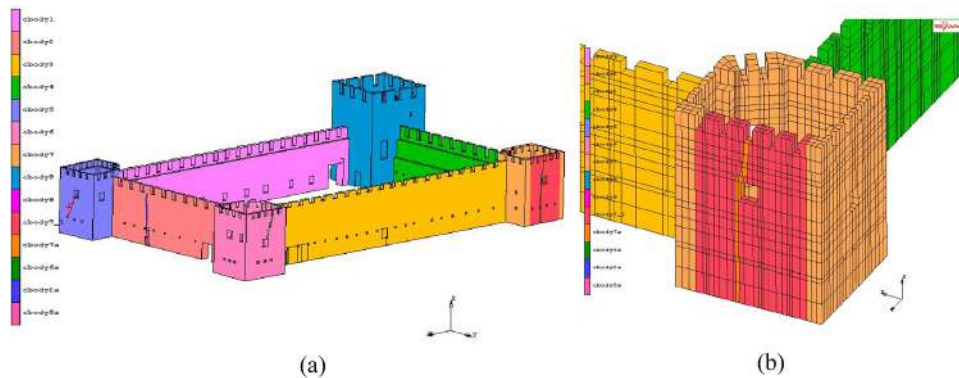


Figure 20 (a) Contact bodies from which the finite element model consist and (b) modelling of major crack of NW tower (see online version for colours)



Between the flexible contact bodies which represent the different parts of the structure (perimeters walls, towers, see Figure 20(a)) fixed conditions were considered. The consideration that not unilateral contact phenomena between walls and towers will be developed based on the absence of significant cracks at the connections to the structure. The technique of flexible contact bodies was used to describe the cracks (like the major crack at the NW tower which is shown in Figure 20(b)) assuming that across these interfaces separation and friction effects are considered.

4 Finite element analysis: results

4.1 Eigenmode analysis

To evaluate the behaviour of the structure under seismic excitations the natural frequencies and the modes of the various models were initially, calculated. The eigenproblem was solved by the Lanczos method that is considered to be one of the best available methods for large-scale structures. The first seven and the 11th normal modes of the construction are shown in Figure 21. From the results, it is concluded that in first frequency the south wall is vibrated and then the others walls follow. The first tower is vibrated at the 11th frequency. It must be noted that at the south and the northwest tower major damages exist.

To determine the number of modes that affect the dynamic behaviour of the structure, the diagrams of effective modal mass and the diagrams of participation factors, in movement and rotation about the x -/ y -/ z -axis were created as shown in Figures 22 and 23. If the effective masses of all modes are added in any particular direction, then the sum gives the total mass of the model, except for mass at kinematically restrained degrees of freedom. The participation factors are defined for the translational degrees of freedom and for rotation around the centre of rotation. From these diagrams, it appears that mass participation can be significant up to a large number of modes, ~200–250.

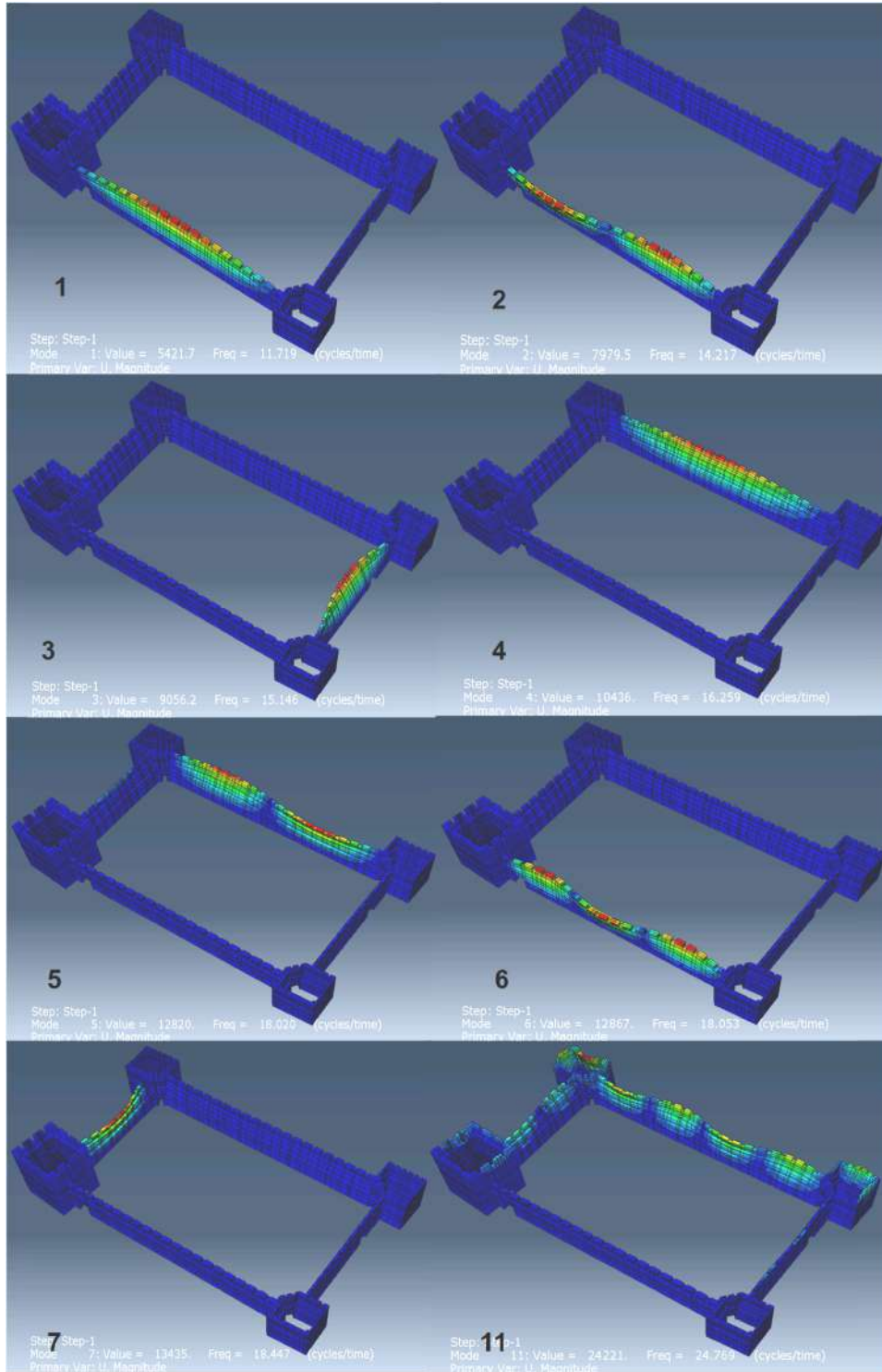
4.2 Spectral analysis

For the spectral analysis, the design spectrum was created, according to the Greek Regulation, which is in accordance with Eurocode 6 (Figure 24). The main assumptions for the creation of this spectrum can be summarised to:

- selection of smaller eigenperiod T_1 compared with the value proposed by the Regulation, in order to widen the spectrum width to the left, since low first eigenperiod is calculated from the analysis and special problems are presented to subsoil
- adoption of value 1 for the behaviour factor, because of the monument's importance
- enlargement of the range from the regulation by a factor of 1.25, because of the proximity to tectonic faults of structure (apparent the subsoil study).

The first assumption was made taking into account the results of modal analysis, such as the fact that the first, fourth, sixth and other modes concerning the oscillation of the south wall and correspond to periods of less than T_1 defined by the Regulation on this case soil. This approach perhaps overestimates the figures for short periods, but it is appropriate to take the peculiarities of this monumental structure (stiffness, pathology, etc.).

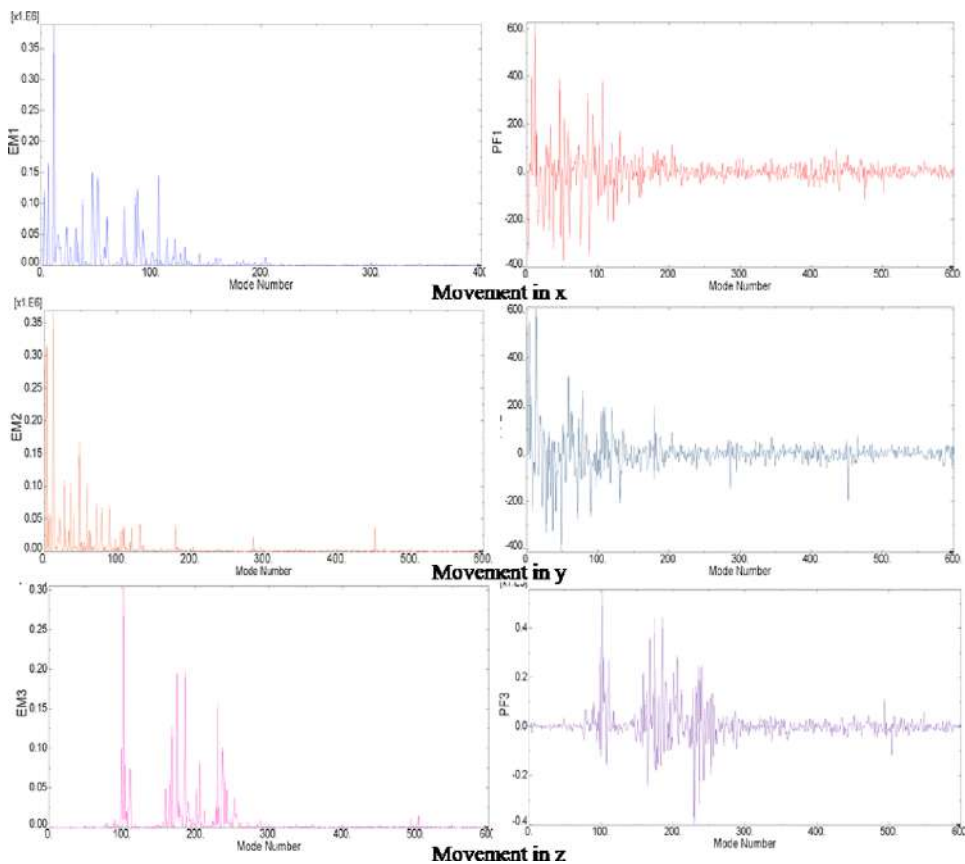
Figure 21 The first seven and the 11th normal modes (see online version for colours)



Additionally, the analysis took into account the 1000 first modes. Finally, the range of values was multiplied by a factor of 1.4, in order to implement the worst load by earthquake in Eurocode 1.

For the analysis, earthquake in three directions in space was considered. The analysis showed that critical case is when the earthquake has north south direction (while reduced participation in other directions). As can be seen from the shapes where the maximum principal stresses are shown (Figures 25 and 26), the critical areas are located in areas where the monument presents failures.

Figure 22 The effective modal mass (EM) and the participation factor (PF) in movement about the $x/y/z$ axis (see online version for colours)



4.3 Non-linear analysis of the structure

The present study is completed with a non-linear dynamic analysis, with direct integration in time of the equations of motion. The accelerograms of three seismic events were selected in order to match to the data of the castle area, to the extent feasible. Moreover, for each phenomenon two analyses were conducted: in the first the accelerogram in x is applied to the x -direction of the vector and the accelerogram in y is applied to the y -direction of the vector. Therefore, the core was tested for $3 \times 2 = 6$ seismic excitations, in total.

Figure 23 The effective modal mass (EM) and the participation factor (PF) in rotation about the $x/y/z$ axis (see online version for colours)

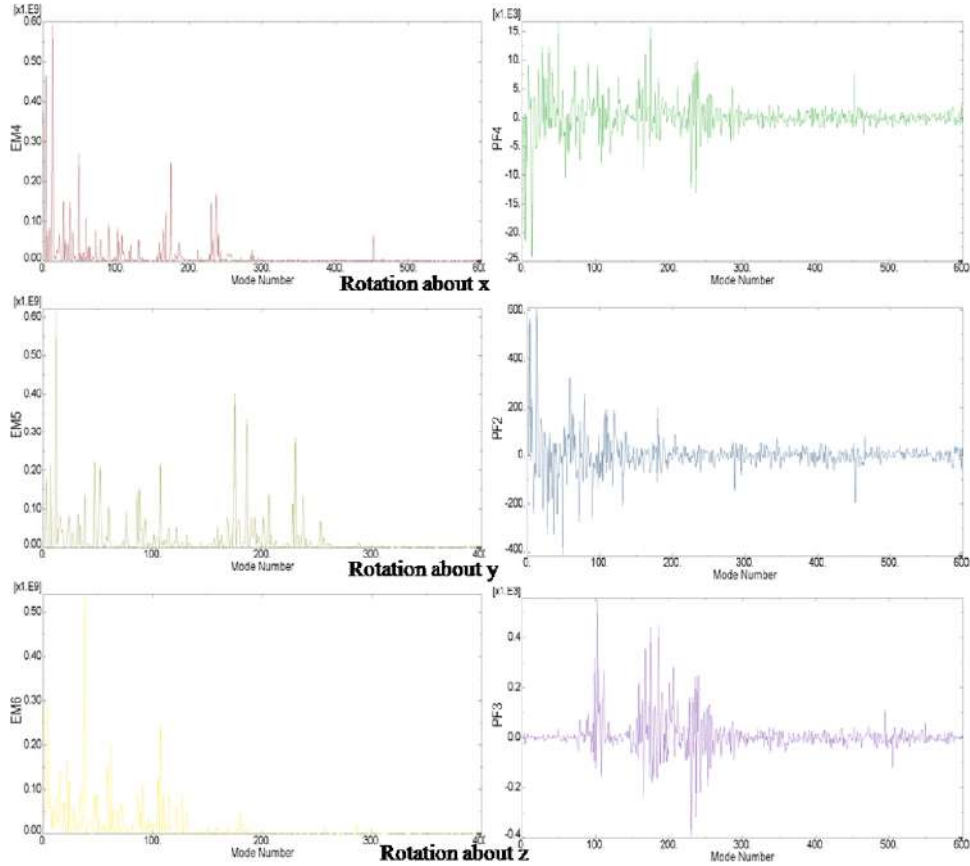
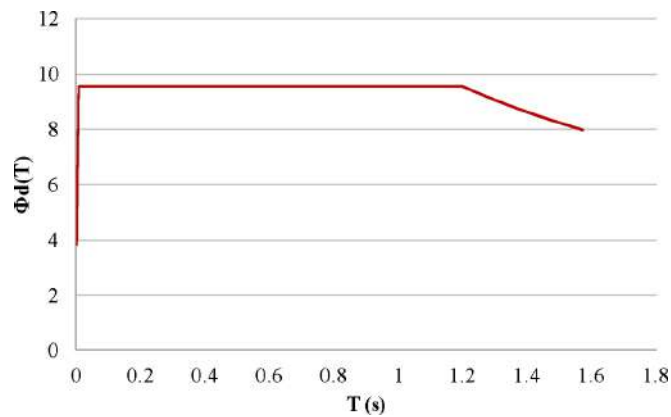


Figure 24 The design spectrum (see online version for colours)



To display any failure of the vector, the non-linear law of fracture (damage) was used. In terms of this law, the non-linear law of stress-strain for both tensile and compressive behaviour was adopted, according to previously mentioned information.

Figure 25 Maximum principal stressed (Pa) at the end of spectral analysis (northeast view) – Model 1 (see online version for colours)

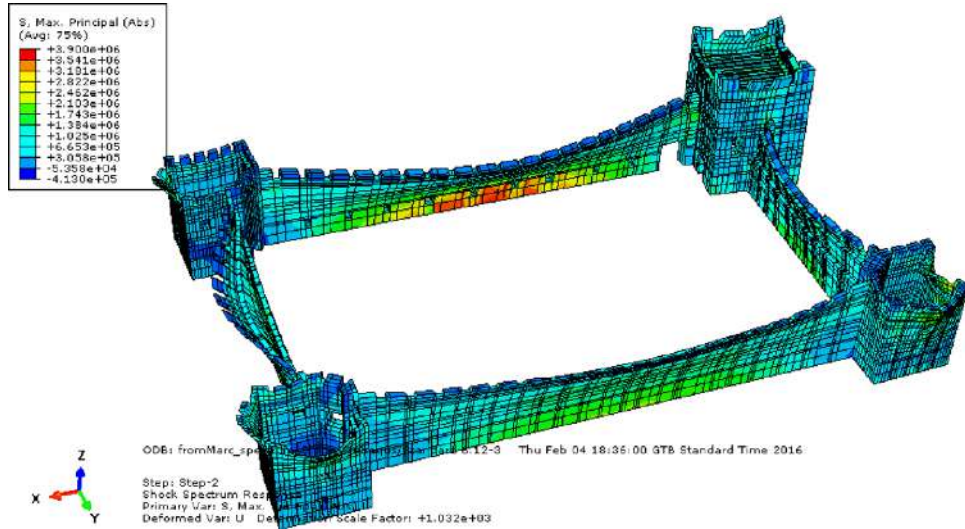


Figure 26 Maximum principal stressed (Pa) at the end of spectral analysis (northwest view) – Model 2 (see online version for colours)

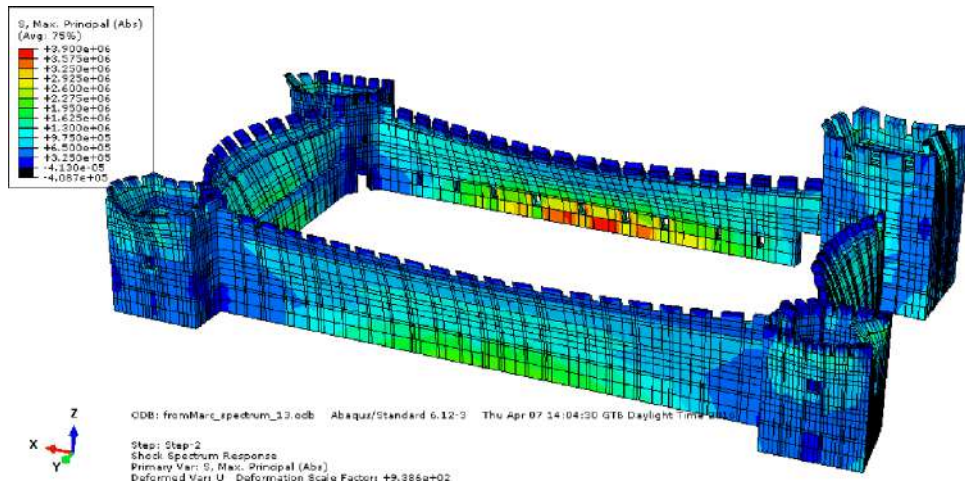


Table 5 Characteristics of seismic events

<i>a/a</i>	<i>Earthquake</i>	<i>Earthquake magnitude</i>	<i>Accelerometer distance from the epicenter (km)</i>	<i>Soil category in Eurocode 8</i>	<i>Peak ground acceleration (g)</i>
1	Northridge, California, 1994	6.69	25.42	B	0.25
2	Irpinia, Italy, 1980	6.69	30.35	B	0.29
3	Kobe, Japan, 1995	6.90	20.00		0.80

Figure 27 Contour plot of equivalent plastic strains of Model 1 and earthquake Kobe_xy (see online version for colours)

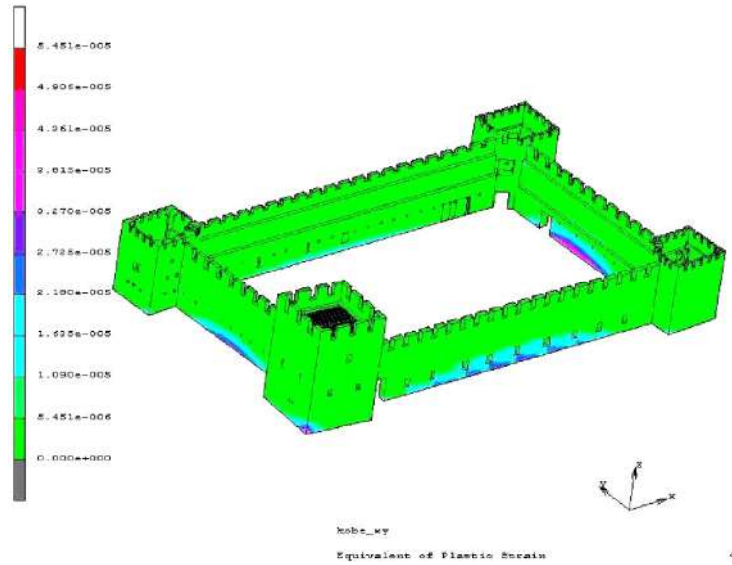
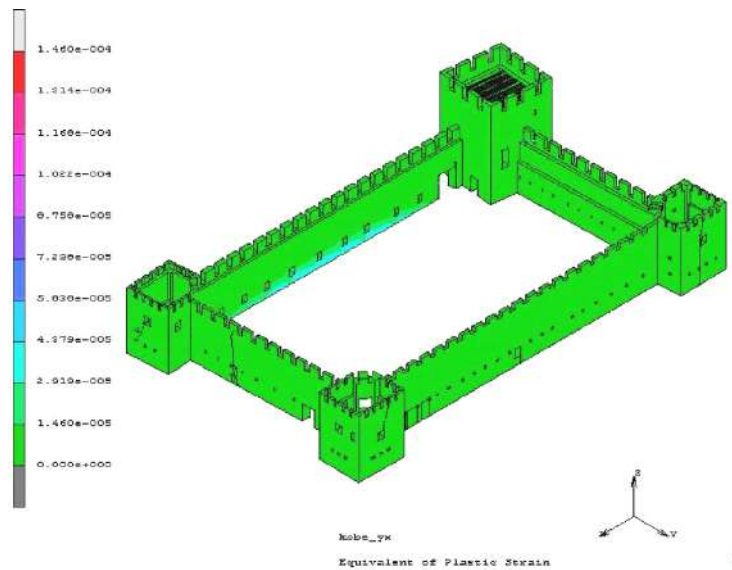


Figure 28 Contour plot of equivalent plastic strains of Model 4 and earthquake Kobe_yx (see online version for colours)



The characteristics of earthquakes and the accelerograms that were selected are depicted below in Table 5. In terms of the analysis, seismic excitation was applied in three directions (x, y, z) of the structure.

As failure indication, the maximum stress criterion (MSC) was used which is based on the calculation of nine failure indices F at each integration point. The nine failure indices are given by

$$F_i = \left(\frac{S_i}{f_{td}} \right) \text{ if } S_i > 0, i = x, y, z$$

$$F_j = \left(\frac{S_j}{f_{cd}} \right) \text{ if } S_j < 0, j = x, y, z$$

$$F_{ij} = \left(\frac{S_{ij}}{f_{sh}} \right), i \neq j, i, j = x, y, z$$

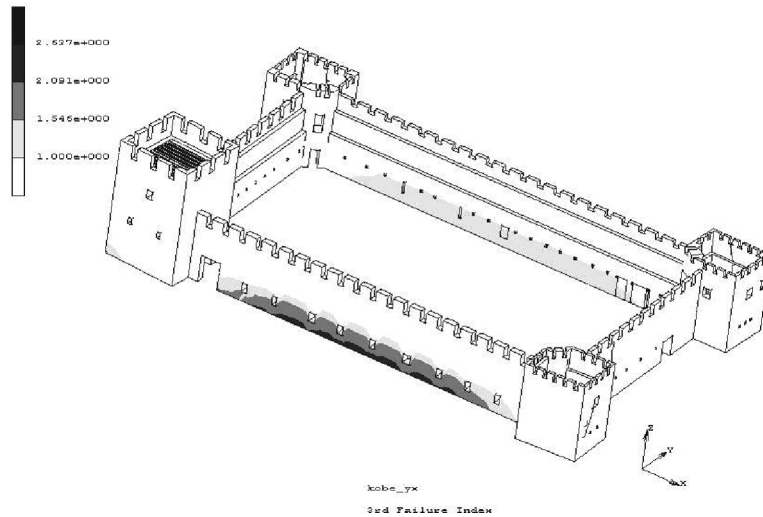
where f_{td}, f_{cd} are the maximum allowable stresses in tension and compression; S_i are the stresses in tension, in x -, y - and z -direction; S_j are the stresses in compression, in x -, y - and z -direction; S_{ij} are the shear stresses in the three planes xy , yz and xz ; f_{sh} is the maximum allowable shear stress.

For the damage criterion, principal tension damage model was used which assumes that damage will occur under conditions of high tensile stress. The damage value is expressed by the formula (MSC.Marc Mentat, 2008):

$$\int \frac{S_{\max}}{\bar{\sigma}} dt$$

where S_{\max} is the maximum (critical) principal stress and $\bar{\sigma}$ is von Mises stress.

Figure 29 Contour plot of 3rd failure index (maximum 2.627) of Model 4 and earthquake Kobe_yx (time step 11.5)



4.3.1 Results of non-linear analysis

In the case with the elastoplastic material model, the estimation of the region with plastic strain is an indication of failure and crack development. In Figures 27 and 28, the contour plots of equivalent plastic strains are shown. The main cracks and the activation of unilateral contact between parts of the cracks lead to increase of plastic strains at the base of south wall, the place where serious faults exist.

Figure 30 Contour plot of damage index (maximum 1.351) of Model 1 and earthquake Kobe_yx at final time step (see online version for colours)

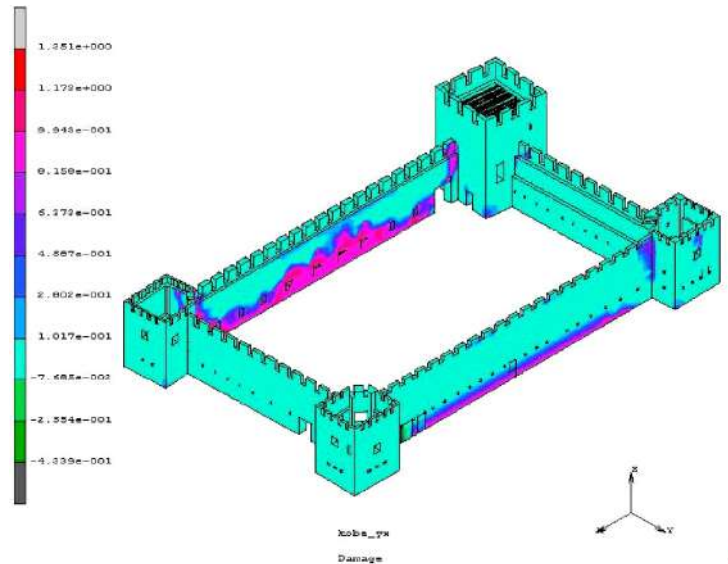
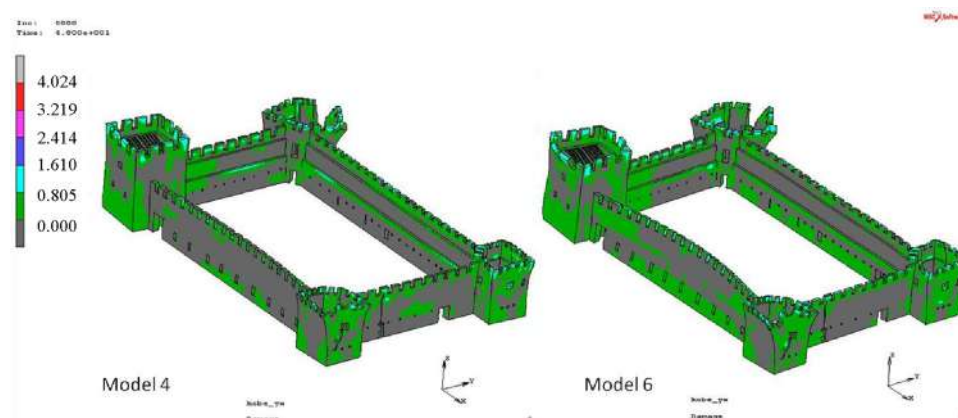


Figure 31 Contour plot of damage index for Models 4, 6 and earthquake Kobe_yx at final time step (see online version for colours)



The reduction of friction coefficient and separation stress across the contact interfaces leads mainly to failures at the base of south wall and north wall as it is shown from Figure 29. The third failure represents the percentage of the maximum allowable stress in tension, in z -direction.

Damage index is an indication of regions where the developed stresses are higher than the permission limits. These areas are critical for possible cracks and materials faults. In Figures 30–32, the contour plots of damage index are given for earthquake Kobe as base excitation. The base excitation was applied in two cases, first was applied main in x -direction (east–west direction of the structure) and parallel in y -direction the same earthquake with an intensity of 60% of the initial (Kobe_xy). In the second case, the excitation had as principal the y direction (north–south) and in the other direction (x)

the same earthquake with an intensity of 60% of the initial are applied (Kobe_yx). From the results of the analysis it was shown that the more critical was the second case (Figure 30). The first case was critical to the vibration of the north wall of the north-west tower. The activation of cracks, at the first time steps of the analysis, acts as mechanism of energy dissipation leading to reduction of the vibration to the structure (Figure 33). When cracks open and no friction mechanism exists the mechanism of energy leads to appearance of more cracks and faults of the structure at different places (Figures 31, 32, 34 and 35). The same conclusion was extracted from Figure 33 where the out of plane displacement of the top line of southern wall ($Uy(m)$) for the first case (earthquake Kobe_xy) is shown.

Figure 32 Contour plot of damage index of Models 1, 4-6 and earthquake Kobe_yx at time step 11.5 s (see online version for colours)

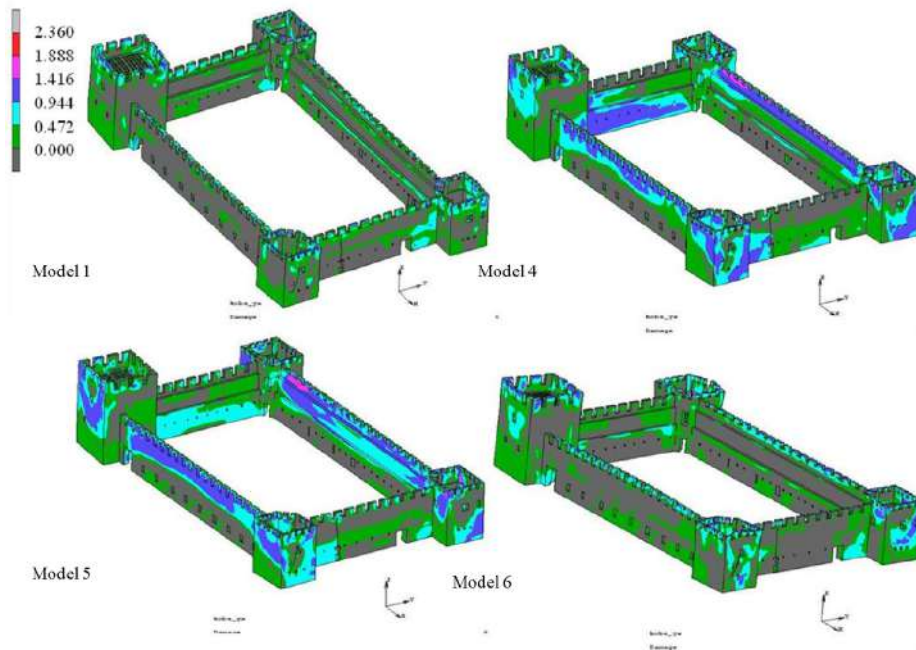


Figure 33 Out of plane displacement ($Ux(m)$) across the top of eastern wall and earthquake Kobe_xy (see online version for colours)

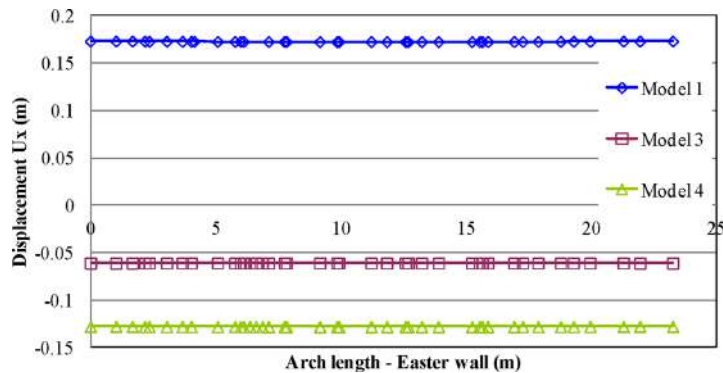


Figure 34 History of the out of plane displacement (U_y (m)) at point C (middle of the top of the north wall of the northwest tower) and earthquake Kobe_yx (see online version for colours)

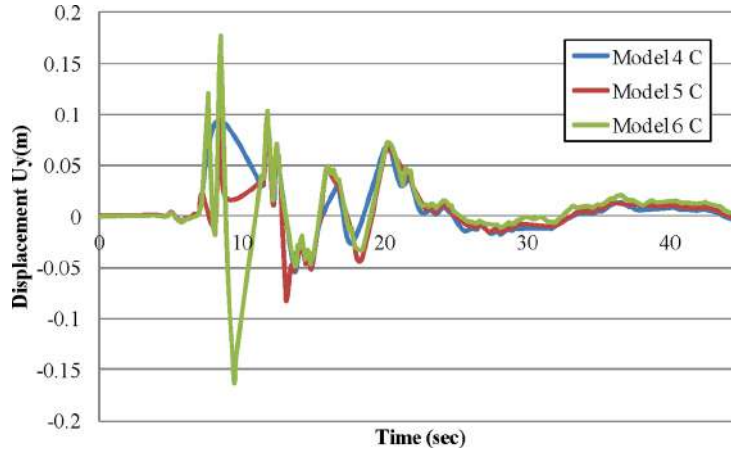
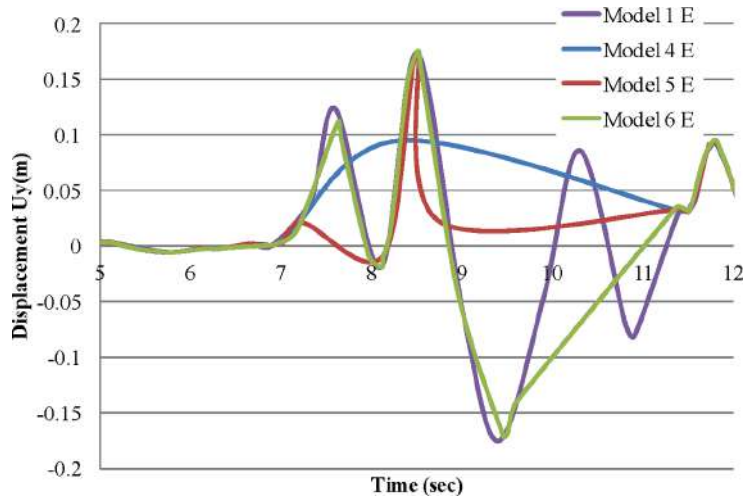


Figure 35 History of the out of plane displacement (U_y (m)) at point E (middle of the top of the north wall of the north-eastern tower) and earthquake Kobe_yx (see online version for colours)



The history of the out of plane displacement for two points, C (middle of the top of the north wall of the northwest tower) and E (middle of the top of the north wall of the north-eastern tower) are given in Figures 34 and 35, for the second case of base excitation (Kobe_yx). The activation of cracks as it was modelled by the unilateral contact interfaces, leads to variation of the structural vibration. If the existing cracks remain without any strengthening, after the excitation of new earthquakes, new cracks will be developed which in combination with the old ones would lead to destroy of the structure.

The mechanism of crack opening and closing is shown in Figure 36 for three indicative points of the cross section of the main crack at the North West tower. Contact status is an indication of the condition between the two contact bodies where

their interface represents the existing crack. When contact status is 0 means that two bodies are not in contact and when its value is 1.0 mean that two bodies are in contact (Figure 37).

Figure 36 History of separation at three indicative points of the cross section of the main crack at the North West tower (see online version for colours)

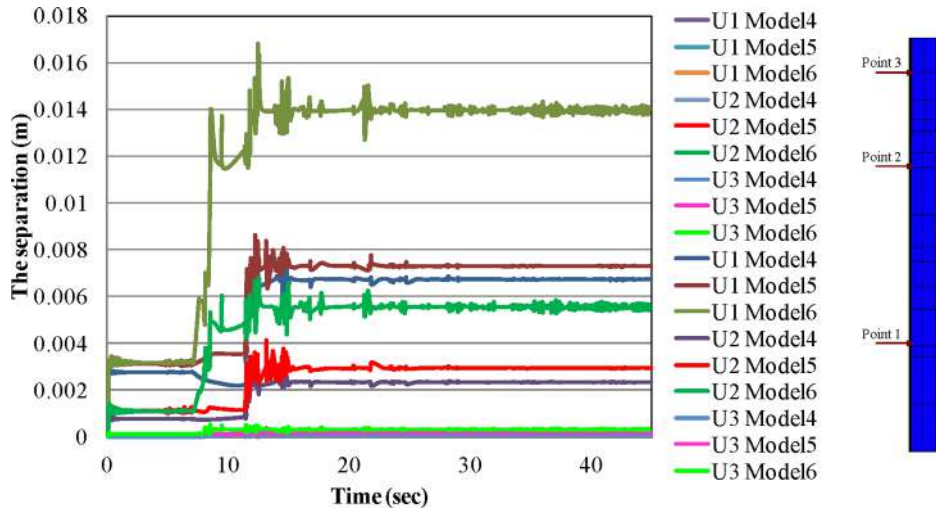
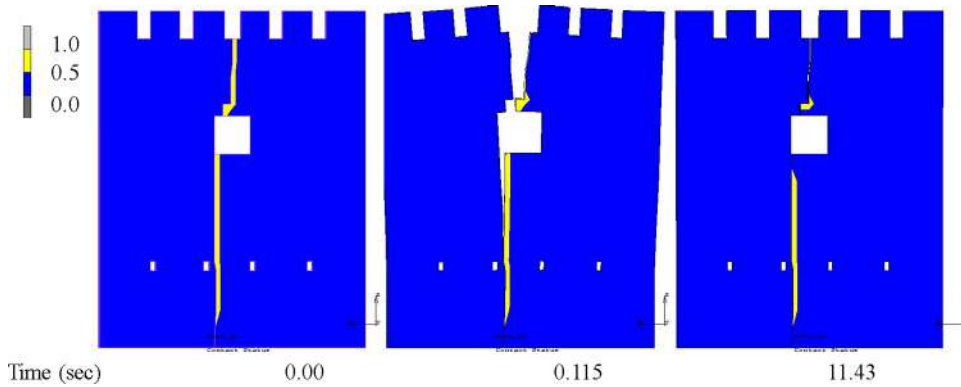


Figure 37 Contact status at three time steps of the main crack at the North West tower (see online version for colours)



5 Conclusions

The FEM is used for the structural analysis of Frangokastello fortress which is in the area of southern Crete. The modelling was based on surveys of existing geometry, history of the monument and interventions have been made, the quality of building materials and subsoil conditions. Especially, existing cracks and faults like disorganisation of the material considered by a reduced modulus of elasticity and cracks were simulated by the technique of unilateral contact interfaces between contact bodies. Smaller faults were not considered to our analysis since they does not affect significant to the mechanical

behaviour of this stiff structure with large enough wide of the walls. Since the quality control of the structure and the finite element analysis, the following conclusions occur:

- 1 The large, bright, vertical crack in the entire height of the north face of the northwest tower is a risk factor for the tower. In likely seismic phenomenon could lead to collapse to part of the tower.
- 2 The northwest tower vibrates at the first frequencies of the structure as shown by the modal analysis. This compared with the previous conclusion lead to the need of strengthen measures which should be taken this tower.
- 3 The disorganisation of the wall in the centre of the south wall appears to be due to out of plane bending after seismic phenomenon. This failure mode is confirmed by the non-linear analysis, under actual earthquakes. In parallel, the south wall is vibrated at the first frequency as shown by the modal analysis.

From modal analysis, the main frequencies of the structure were calculated in order to estimate the frequencies which activate mainly the structural vibration. From spectral analysis, the critical areas are located in areas where the monument presents failures. The non-linear analysis was done for different earthquakes which were selected to match to the data of the castle area, to the extent feasible. More critical results were extracted for the Kobe earthquake with the maximum peak ground acceleration.

The choices on the restoration materials and architectural interventions regarding the structure of our fortress were mainly determined by the principles of relevance and compatibility with the totality of meanings of the historical process. For the restoration of the structure the main interventions which were proposed are:

- The masonry cracks will be filled with new mortar reinforced and secured with stainless steel staples.
- The areas where original material was removed in depth, along with parts of the original masonry at the bottom of the small towers will be restored. The vault of the SE tower will be completed to roof the ground floor.
- The barrack rooms and towers will be roofed and the intervening floors will be constructed of frames of Greek chestnut, connected to the walls. These connections have been designed as free joints (elastic connection), to avoid pounding phenomena between the two structures which will have different materials.
- All areas with total or partial loss of masonry or weathered cement mortar will be replaced by new repair material.

Pierdicca et al. (2016) proposed the use of wireless sensor networks (WSN) as a new kind of architecture for structural monitoring systems. They presented the main results obtained in the context of the '*Palazzo Comunale di Castelfidardo*' monitoring project with WSN, with the aim to get an accurate numerical model that simulates the dynamic behaviour of the whole structure. In the future a system for structural health monitoring of our structure would be used to improve our numerical model and to control the effectiveness of the strengthening solutions which are proposed. In parallel for future research, more earthquakes could be considered with different characteristics. Additional, the parametric investigation of the parameters which were considered for structural

failures and cracks would also extend this research in parallel with experimental investigation.

Acknowledgements

This research was funded by the research program with title ‘Frangokastello Sfanion: Investigation of wears - Rehabilitation – Proposals for usage and for promotion of the monument’. Programming cultural development contract for the research program between the Region of Crete – the Municipality of Sfakia –Ephorate of Antiquities of Chania and the University of Crete (2015).

References

- Betti, M., Drosopoulos, G.A. and Stavroulakis, G.E. (2008) ‘Two non-linear finite element models developed for the assessment of failure of masonry arches’, *Comptes Rendus Mécanique*, Vol. 336, Nos. 1–2, pp.42–53.
- Betti, M., Orlando, M. and Vignoli, A. (2011) ‘Static behaviour of an Italian medieval castle: damage assessment by numerical modelling’, *Computers and Structures*, Vol. 89, pp.21–22.
- Cattari, S., Abbati, S.D., Ferretti, D., Lagomarsino, S., Ottonelli, D., Tralli, A. (2014) ‘Damage assessment of fortresses after the 2012 Emilia earthquake (Italy)’, *Bulletin of Earthquake Engineering*, Vol. 12, No. 5, pp.2333–2365.
- Cheimonas Th., Manoutsoglou E., Stavroulaki M. and Skoutelis N. (2016) ‘Classification of building stones of the Frangokastello Castle, Sfakia, Crete’, *Proceedings of the 14th Intern. Congress, Bulletin of the Geological Society of Greece*, Thessaloniki, May, Vol. L, pp.209–217.
- Ford, T.E., Augarde, C.E. and Tuxford, S.S. (2003) ‘Modelling masonry arch bridges using commercial finite element software’, *Proceedings of the 9th International Conference on Civil and Structural Engineering Computing*, Civil Comp Press, Paper 101, Holland, Stirling.
- Leftheris, B.P., Stavroulaki, M.E., Sapounaki, A.C. and Stavroulakis, G.E. (2006) *Computational Mechanics for Heritage Structures*, WIT Press, Boston.
- Lourenço, P.B. (2002) ‘Computations on historic masonry structures’, *Progress in Structural Engineering and Materials*, Vol. 4, pp.301–319.
- MARC Analysis Research Corporation (1997) *Theory and User Information*.
- Milani, G., Esquivel, Y.W., Lourenço, P.B., Riveiro, B. and Oliveira, D.V. (2013) ‘Characterization of the response of quasi-periodic masonry: geometrical investigation, homogenization and application to the Guimarães castle, Portugal’, *Engineering Structures*, Vol. 56, pp.621–641.
- Milani, G., Sanjust, C.A., Casolo, S. and Taliercio, A. (2012) ‘Maniace castle in Syracuse, Italy: comparison between present structural situation and hypothetical original configuration by means of full 3D FE models’, *The Open Civil Engineering Journal*, Vol. 6, Sp. Issue No. 1, pp.173–187.
- MSC.Marc Mentat (2008) *Theory and User Information*.
- Pierdicca, A., Clementi, F., Isidori, D., Concettoni, E., Cristalli, C. and Lenci, S. (2016) ‘Numerical model upgrading of a historical masonry palace monitored with a wireless sensor network’, *International Journal of Masonry Research and Innovation*, Vol. 1 No. 1, pp.74–99.
- Spyrakos, C.C. (1995) *Finite Element Modeling in Engineering Practice*, Algor Publishing Division, Pittsburgh, PA.

- Stavroulaki M.E. (2004) 'Finite element analysis of a stone bridge for failure prediction', *Proceedings of the 7th National Congress on Mechanics*, 24–26 June, Chania, Crete, Greece, pp.38–43.
- Stavroulaki, M.E. and Liarakos, V.B. (2012) 'Dynamic analysis of a masonry wall with reinforced lintels or tie beams', *Engineering Structures, Elsevier*, Vol. 44, pp.23–33.
- Stavroulaki, M.E. and Stavroulakis, G.E. (2002) 'Unilateral contact applications using FEM software', *Intern. Journal of Applied Mathematics and Computer Sciences, Special Issue on 'Mathematical Modeling and Numerical Analysis in Solid Mechanics'*, Vol. 12, No. 1, pp.101–111.
- Stavroulaki M.E., Sapounaki A.K., Leftheris B.P., Stavroulakis G.E. (2002) 'Nonlinear finite element for damage analysis of the Plaka stone bridge in Epirus', Tsahalis, D. (Ed.): *GRACM 2002: Proceedings of the 4th Hellenic Conference of Computational Mechanics*, University of Patras, Greece, 27–29 June, CD-ROM.
- Tassios, T.P. and Chronopoulos, M.P. (1986) 'A seismic dimensioning of interventions (repairs/strengthening) on low-strength masonry building', *Middle East and Mediterranean Regional Conference on Earthen and Low-Strength Masonry Buildings in Seismic Areas*, Ankara, August–September.
- Tiberti, S., Acito, M. and Milani, G. (2016) 'Comprehensive FE numerical insight into Finale Emilia Castle behaviour under 2012 Emilia Romagna seismic sequence: damage causes and seismic vulnerability mitigation hypothesis', *Engineering Structures*, Vol. 117, pp.397–421.